Received 7 February 2023; revised 13 March 2023; accepted 29 March 2023. Date of publication 3 April 2023; date of current version 12 April 2023.

Digital Object Identifier 10.1109/OJAP.2023.3264250

3-D Printed Dually Symmetric Orthomode Transducer and Horn Antenna at X-Band

IAN GOODE AND CARLOS E. SAAVEDRA

Department of Electrical and Computer Engineering, Queen's University, Kingston, ON K7L 3N6, Canada

CORRESPONDING AUTHOR: I. GOODE (e-mail: ian.goode@queensu.ca)

This work was supported in part by the Natural Sciences and Engineering Research Council of Canada (NSERC) under Grant RGPIN-2022-05204.

ABSTRACT A dually symmetric orthomode transducer (OMT) and horn antenna are presented for both single port linearly polarized operation and dual port circular polarization use. The feed uses two waveguide splitters and a feed bend to feed a four-port horn antenna that has the two groups of ports orthogonal to each other to produce a symmetric radiation pattern. The feed is printed from 316L stainless steel while the horn is printed from a plastic polymer and metallized using aluminum tape. The structure is based on WR 90 waveguide and covers the guide's full operating band of 8.2 GHz to 12.4 GHz. Peak realized gain values of 20.5 dBi were measured with cross polarization rejection of over 40 dB. Here linearly polarized and circularly polarized results are presented, the latter using an off-the-shelf hybrid to control the phase for the two ports. Enabled by the symmetric feed, both the linear and circularly polarized radiation patterns were highly symmetric.

INDEX TERMS 3D printing, additive manufacturing, circular polarization, horn antenna, linear polarization, orthomode transducer, waveguide, x-band.

I. INTRODUCTION

THE ABILITY to combine two orthogonally polarized signals into a common antenna is necessary for multiplexing of linear signals or creating circularly polarized signals. In waveguides, this combination of two linearly polarized orthogonal paths into a common guide or antenna is often referred to as an orthomode transducer (OMT), where two orthogonal rectangular waveguides are combined into a common square or circular waveguide. These types of structures have been made in both traditional waveguide and substrate integrated waveguide topologies [1], [2], [3], [4], [5], [6], [7], [8], [9], [10], [11], [12], [13]. These OMTs combine two or more waveguide paths into a common waveguide by bending orthogonal guides together [9], using a series of matching structures [4], [7], [8], probe feeding a horn from multiple points [12], through waveguide turnstiles [1], [2], [3], [6], [10], or other balanced structures [5], [13] where the common waveguide is fed symmetrically with pairs of single polarization waveguides.

Most OMT structures rely on an asymmetric feed to combine two orthogonally polarized paths into a common waveguide. However, this asymmetric feed can result in an asymmetric ration pattern this was observed in [8] where two rectangular waveguides were brought into the corner of a horn antenna, or in [9] where two orthogonal paths were bent together, both producing asymmetric far-field patterns. Waveguide turnstiles, among other applications like circulators, can be used to combine two orthogonally polarized paths into a common guide in a balanced fashion [1], [2], [6], [10], [11], [14], [15], [16], [17]. These types of structures feed each of the co-polarized paths with a power divider and phase matched lengths of waveguide to create a two port device (one for each of the orthogon paths) that feeds the common guide with symmetrically. These types of structures are difficult to machine and require CNC machining out of multiple parts [2], [6], multi-layer substrate integrated waveguide structures [1], or to be fabricated as a monolithic structure using additive manufacturing [10], [11].

Besides subtractive CNC machining or PCB fabrication methods, additive manufacturing has been used to create waveguide components. Multiple types of additive manufacturing with different materials can be used. Recently, waveguide components have been printed using metal processes such as direct metal laser sintering (DMLS) where a metal allow powder is sintered into the shape of a desired structure [10], [11], [12], [13] or through fused deposition

modeling (FDM) that forms the structure out of plastic and then the components are metallized using metal foil tapes or conductive paints [9], [18], [19]. The metal printing options allow for monolithic structures that are difficult machine through traditional operations or would require many different setups or be fabricated from multiple parts that do not require significant post processing. These types of structures can be used without additional steps to electroplate or smooth the structures. These have been seen for waveguide OMTs and multi-feed horns from microwave frequencies [12], [13] to mm-wave frequencies [11]. Since these parts are fabricated from metallic alloys they often weigh as much as traditionally machined parts. However, the additive manufacturing process makes it possible to build geometrically complex parts that are difficult to make through subtractive manufacturing methods. The FDM printed and metallized waveguide options are comparatively much lighter and more cost-effective as FDM printing is considerably less expensive and more readily available than DMLS printing processes while still being able to offer comparable performance to CNC machined or DMLS printed waveguide structures.

This work presents a symmetrically fed OMT and horn that can be used for wide-band polarization division multiplexing or for transmitting or receiving circularly polarized signals when each port of the antenna is appropriately fed. This antenna is a two port device where each feed port is split into two paths that are symmetric about the center axis of the antenna. The two groups of waveguide paths are orthogonal to each other and are separated by a pyramid in the center of the horn. Using a topology that employed symmetry and equal physical length paths that is simpler to design than other symmetric feeds such as waveguide turnstiles. The feed structure is fed by off-the-shelf WR 90 launchers and the path division and combination is accomplished through custom DMLS printed waveguide dividers. The recombination of the four paths is accomplished in the horn antenna without the need for a turnstile or other waveguide structure. The complex geometry of the waveguide paths was achieved using DMLS a process that selectivity sintered powered 316L stainless steel into a solid structure that provided usable performance with minimal post-processing. The structure of the horn was FDM 3D printed from PLA and metallized using aluminum foil tape as the horn was easier to section into multiple parts to allow for the affixation of the aluminum tape. The feed was metal 3D printed rather than CNC machined or FDM printed and metalized since the geometry of combining the four paths made it difficult to section the part for either CNC machining or metallizable FDM printed parts. Metal DMLS printing is considerably less costly compared to CNC machining. This combination of DMLS and FDM printing allowed for a cost and weight optimized system over traditionally machined components.

II. HORN AND FEED DESIGN

The design of this horn and feed was completed using the full-wave electromagnetic simulator ANSYS HFSS.

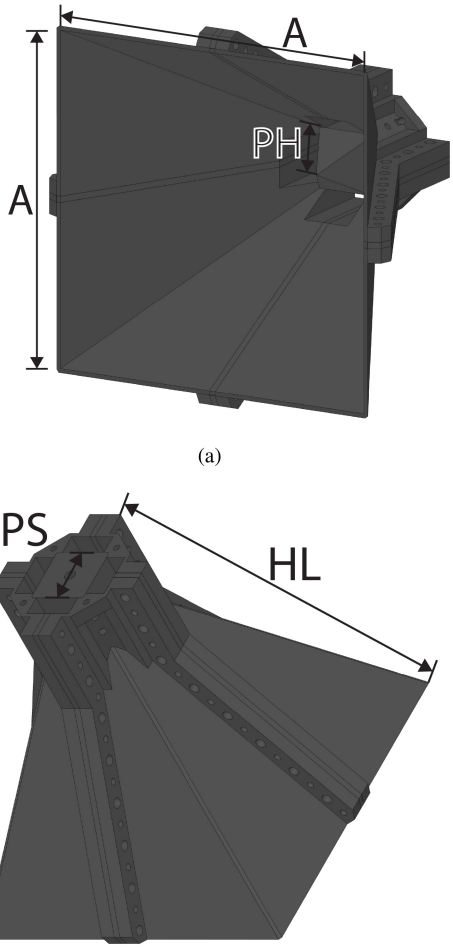

var.	A	PH	PS	HL
[mm]	160.0	27.9	28.9	150.0

FIGURE 1. Full assembly of the horn showing: (a) inside the horn with the center spike dividing the four paths, (b) the flange end of the horn.

Horn Design – The horn in this work was designed to have two orthogonal feeds so that it could be used for circularly polarized signals or polarization division multiplexing with two discrete orthogonal linearly polarized signals. Here the two feeds were mirrored about the center axis of the horn so that each orthogonal feed pair was symmetric. The goal of this design was to produce a symmetric radiation pattern for all use cases rather than an asymmetric pattern that can be seen from an OMT with an asymmetric feed. This horn was fed by four rectangular waveguide ports of the standard WR 90 dimensions as shown in Fig. 1. The separation between the parallel paths PS was chosen to be close to $\lambda_0/2$ to avoid grating lobes within the horn but was made larger than a to allow for sufficient material between each of the paths at the top of the flange. In the situation where $PS = a$ each of the paths would have touched at the corners making the part difficult to manufacture and reduced the isolation between the orthogonal paths. Between the feeding ports inside the horn, a pyramidal structure was used to

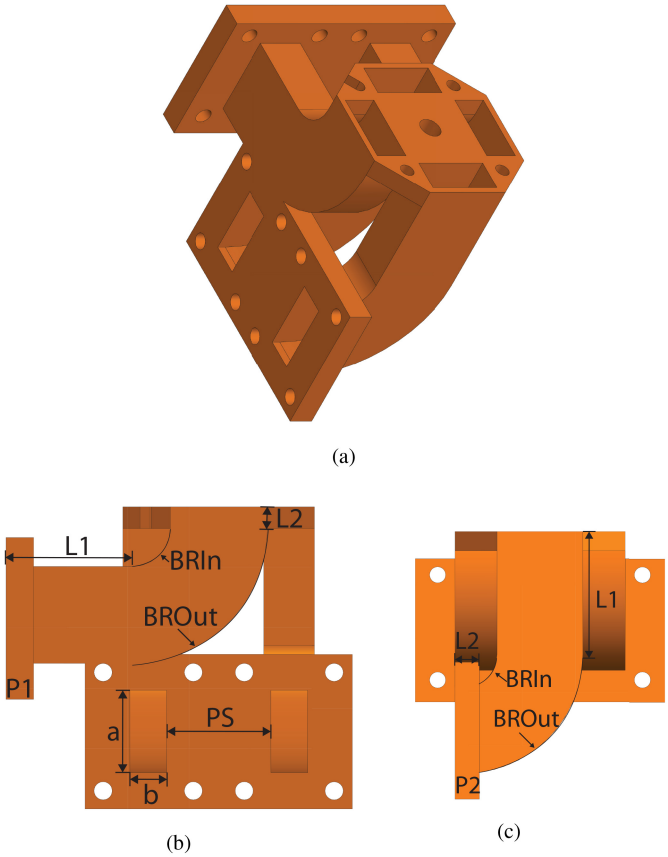

var.	a	b	$L1$	$L2$	$BRIn$	$BROut$	PS
[mm]	22.9	10.2	35.0	6.0	10.5	37.4	28.9

FIGURE 2. Feed bend to combine each feed path into a common flange. (a) Isometric view, (b) Side-view showing the path of port 1, and (c) Side-view showing the path of port 2.

separate the feed ports and increase the isolation between orthogonally polarized ports. The pyramid was designed to have the same slope as the rest of the horn. The overall size of the horn was chosen so that it could easily be printed on a general-purpose FDM 3D printer. The dimensions of the horn were tuned in simulation to improve the impedance match into each port and maximize the port isolation between orthogonally polarized ports.

Feed Design – The feed was designed to be symmetric to avoid any-beam tilt and to match up with the horn designed in Fig. 1, while only being fed from two separate waveguides. To do this, each of the feed paths were split with a waveguide splitter and then bent to have a four-port feed where each set of the parallel waveguides were co-polarized and in phase and the same phase delay was designed on the orthogonal paths. This setup allowed for the horn to produce circular polarization if fed by a 90° hybrid. The feed bend pictured in Fig. 2 shows the series of waveguide bends that combine the orthogonal paths into a common flange. Here each of the paths are the same length as pictured in Fig. 2 (b) and (c) where both paths have the same linear length $L1 + L2$ and the same bend radius. The length $L1$ and $L2$ were chosen so that the

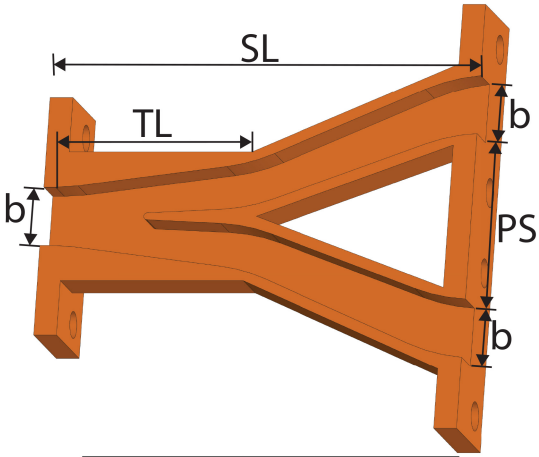

var.	b	SL	TL	PS
[mm]	10.2	75.0	36.0	28.9

FIGURE 3. Sectioned view of waveguide splitter, cut at the mid-point of the $\vec{E}$ wall, the depth of the waveguide normal to the section cut is a constant $a = 22.86mm$ to match the standard WR 90 waveguide dimensions.

mounting flanges would not interfere with the other path. This can be seen in the isometric view in Fig. 2 (a) where the flange for port 2 is flush with the side of the waveguide for the port 1 paths. The bend radius on each bend was chosen to be gentle but still compact as to reduce the total size of the feed bend. The dimensions of the top flange of the feed bend were designed to match up with the spacing of the ports of the horn in Fig. 1.

To feed the parallel paths of the feed bend, a waveguide splitter was made to divide a single WR 90 waveguide into two parallel waveguides. Here the splitter was designed to split the waveguide in the $\vec{E}$ plane. A sectioned view of the splitter is shown in Fig. 3. This splitter gradually increased the height b of the single waveguide and then inserts a divider wall before bending the two paths apart to a path separation of PS to match the port separation of the feed bend in Fig. 2. The final output waveguides are tapered back to be the standard WR 90 size. Here the length of the tapered section at the split TL and the total length of the divider were optimized in simulation for the best impedance match through the divider while keeping the full design compact. The single port divider had a standard WR 90 flange to mate to an off-the-shelf WR 90 launcher, and the opposite flange had mounting holes to match up with the feed bend.

The full assembly of the feed structure is shown in Fig. 4 with the parts separated two emphasize the individual parts from Figs. 2 and 3. Finally, the full system from the waveguide launchers to the horn is shown in Fig. 5.

Fabrication – The horn and feed were fabricated using two different additive manufacturing methods. The horn itself was FDM printed from PLA and metallized using adhesive backed aluminum tape. The feed of the horn was DMLS 3D printed using selective metal sintering which sintered 316L stainless steel into a solid structure. The assembled feed was metal printed in three parts: two waveguide splitters, and a feed

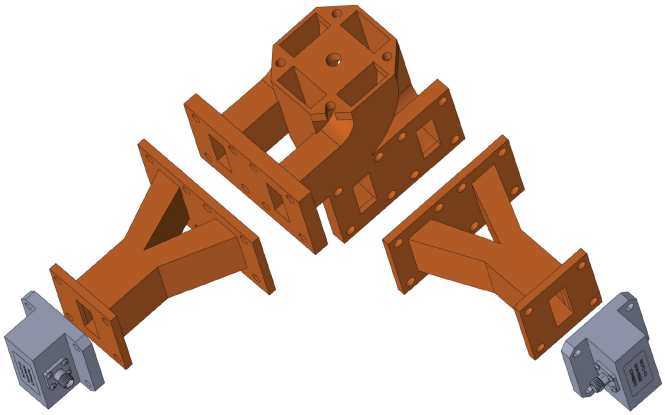

FIGURE 4. Exploded assembly of the waveguide splitters, waveguide launchers, and the feed bend from Fig. 2.

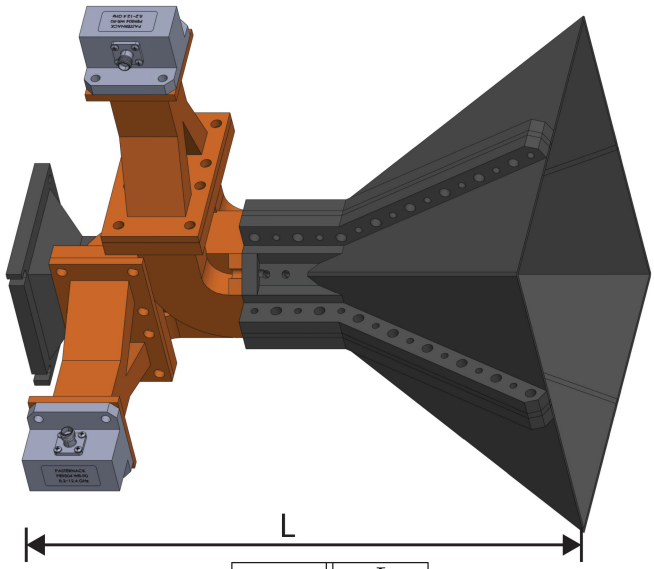

var.	L
[mm]	233.0

FIGURE 5. The full assembly of the horn from Fig. 1 and the feed structure from Fig. 4, the horn, and a printed mount to hold the entire assembly in the measurement system.

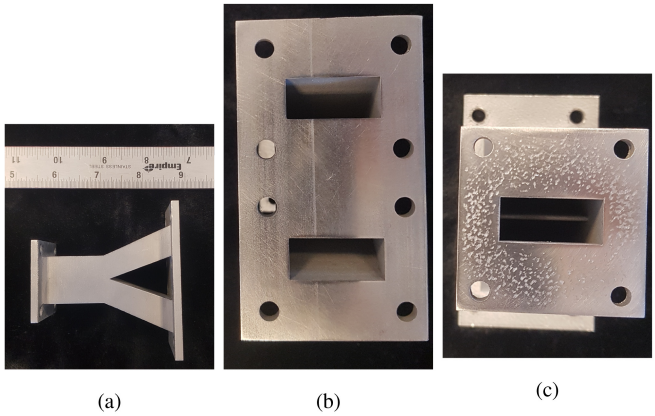

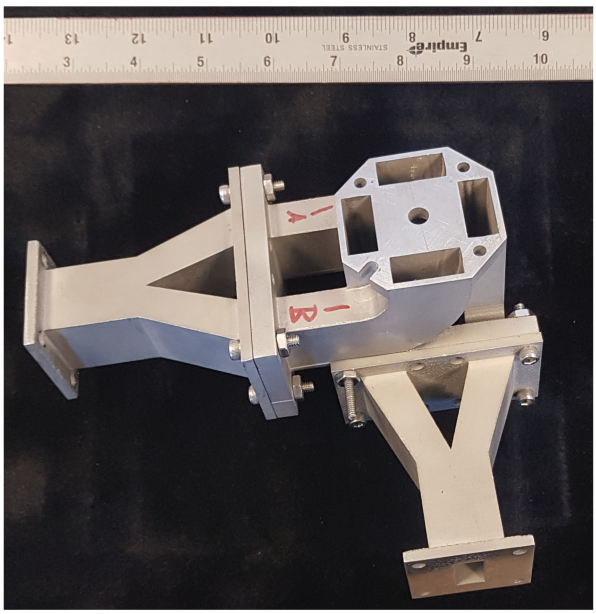

FIGURE 6. Metal 3D printed waveguide feed. (a) Waveguide splitter top view, (b) waveguide splitter end view, (c) waveguide splitter end view, and (d) two waveguide splitters feeding the feed bend. (Ruler in inches for scale).

bend. The assembled feed is shown in Fig. 6. These parts were 3D printed at a commercial print shop from 316L stainless steel. The wall finish was smooth and no post processing was needed on vertically printed walls. The feed was broken into three parts so that the largest number of inner walls could be printed vertically. The horizontally printed surfaces like the waveguide flanges in Figs. 6 (b) and (c) were manually sanded to polish the flange to make the waveguide structures mate with each other and waveguide launchers. After polishing some pitting can still be seen in Fig. 6 (c) however, the waveguide flange was smooth and flat directly around the waveguide where the flush electrical connection is most important. The parts in Fig. 6 were all metal 3D printed rather than metallizing PLA like the horn structure, because the complexity of the feed geometry required it to be partitioned into many small pieces. Once the parts are wrapped in aluminum tape, it is difficult maintain precise alignment between the interconnecting parts which noticeably degrades the performance of the part. For each of these parts, the waveguide paths were printed vertically which allows for the smoothest inner surfaces so that the components can be used without and post-processing. However, because of the bends in the feed structure, some of the paths were printed with horizontal overhangs. This required sacrificial support material inside the waveguide during printing to prevent sagging of the waveguide walls. After the printing was complete, the sacrificial support material was removed and a thin (6.5 mm wide) belt sander was used to smooth and polish the waveguide walls where the support material had been attached. The sanding operation was brief and only a minuscule amount of material was removed. Following the polishing step, the parts were fastened together using bolts and nuts together as seen in Fig. 6 (d).

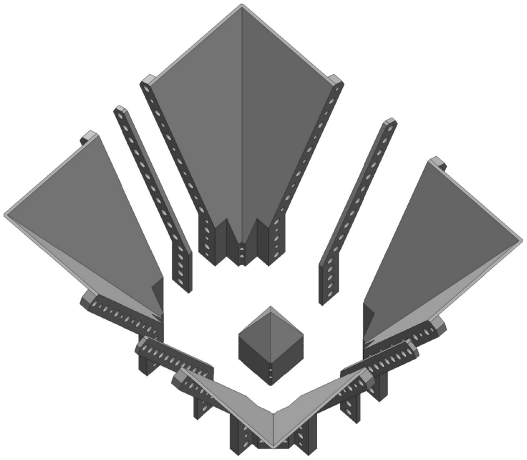

FIGURE 7. Exploded view of the nine parts of the horn to be printed.

The horn was FDM printed in nine sections as shown in Fig. 7, the four corner pieces of the horn, the center separator spike, and the spacers between each corner section (printed in gray in Fig. 8 (b)). The fully printed horn including the full assembly is shown in Fig. 8. The horn was printed with spacers between the corner pieces to allow for the possible addition of ridges. The horn was assembled by taping the holes in the corner pieces to receive an M4 screw. Each piece of the horn was metallized with adhesive backed aluminum tape, and then the horn was assembled. After assembly, additional tape with a conductive adhesive was applied over the seams to improve the electrical connection between all pieces of the horn. The connection between the horn and the feed was made with locating pins in the corners of the horn (the holes for which are shown in Fig. 8 (b)) and the horn was securely to the feed bend using a large bolt up the center of the flange. A large course threaded fastener was used as this allowed the tapped threads in the PLA of the horn to hold more force and increase the mounting pressure. This bolt was also used to secure a mount through the feed bend that was used to mount the full setup in the anechoic chamber.

The fully assembled horn and feed is shown in Fig. 8 (c) without the waveguide launchers. The fabricated mass of the stainless steel feed in Fig. 6 was 1380 g and the mass of the plastic horn was 290 g for a total mass of the configuration shown in Fig. 8 (c) of 1670 g.

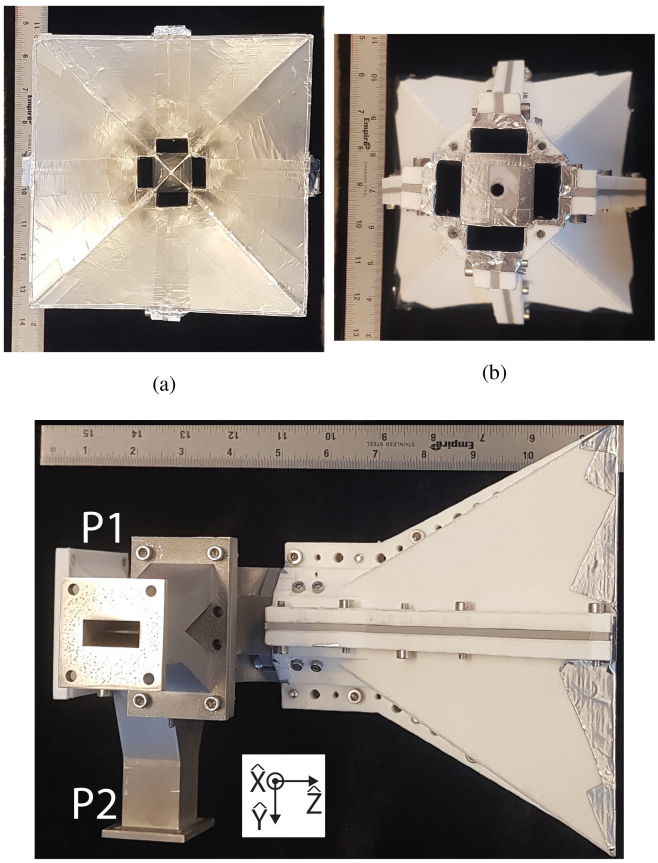

(a) (b) (c)

FIGURE 8. Aluminum tape metallized horn: (a) view looking down the aperture of the horn, (b) view looking at mounting flange for the horn for how the horn mounts to the feed in Fig. 6 (d), and (c) fully assembled horn, feed bend, and waveguide splitters. (Ruler in inches for scale).

III. MEASURED RESULTS

After assembly, the horn was measured to determine its frequency response and radiation characteristics. To match the setups between measurement and simulation, a waveguide calibration was performed that set the reference plane for each port after the coaxial-to-waveguide launcher at the plane of the waveguide flanges seen in Fig. 8 (c). This matched the wave ports that were used to excite the simulation model. This was accomplished using a Anritsu MS4644B vector network analyzer that was calibrated using a WR 90 calibration kit (A-INFO 90CLKA1). Using this calibration setup, the frequency response of the horn was measured and compared to the simulation results. The input reflection (Γ) is presented in Fig. 9 (a) with the port isolation being shown in Fig. 9 (b). For both measurements, the horn was positioned at a wall of absorber in the far-field to minimize any radiation reflections. During the measurement of internal reflection, there was good agreement between measurement and simulation across the full standard operating bandwidth of WR 90 (8.2 GHz to 12.4 GHz). The measured port isolation is higher than expected from simulation but is still below -40 dB for the entire band.

Next, all radiation characteristics were measured in the Queen's University anechoic chamber where the free space and cabling path losses were calculated using a TD HRN-0118 reference horn antenna with ISO17025 calibration accreditation. This allowed the measurement setup to report realized gain across the operating band. First, the two ports of the horn were measured independently to show the linearly polarized operating conditions of the horn. During this, the measured port was connected to the measurement system and the other port was terminated with a matched load. For each port, the measured realized linear co-polarized peak realized gain was reported in Fig. 10 (a) with the linear cross polarization rejection shown in Fig. 10 (b). Both

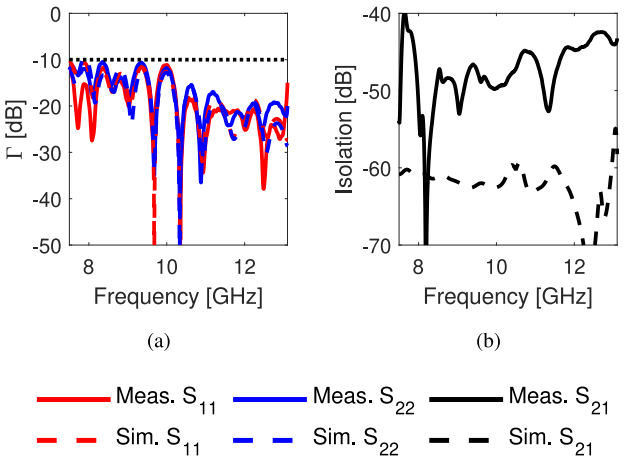

FIGURE 9. Measured and simulated (a) input reflection and (b) port isolation.

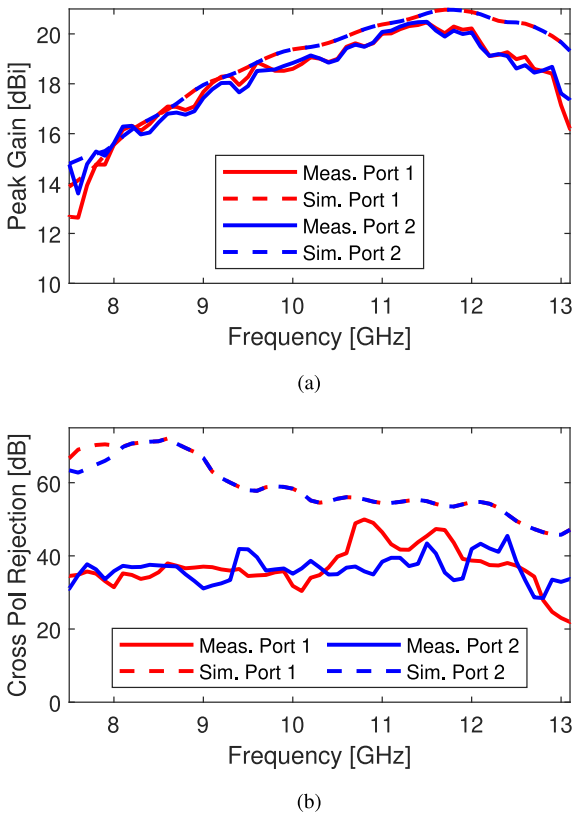

FIGURE 10. Measured and simulated linear (a) peak realized gain and (b) cross polarization rejection.

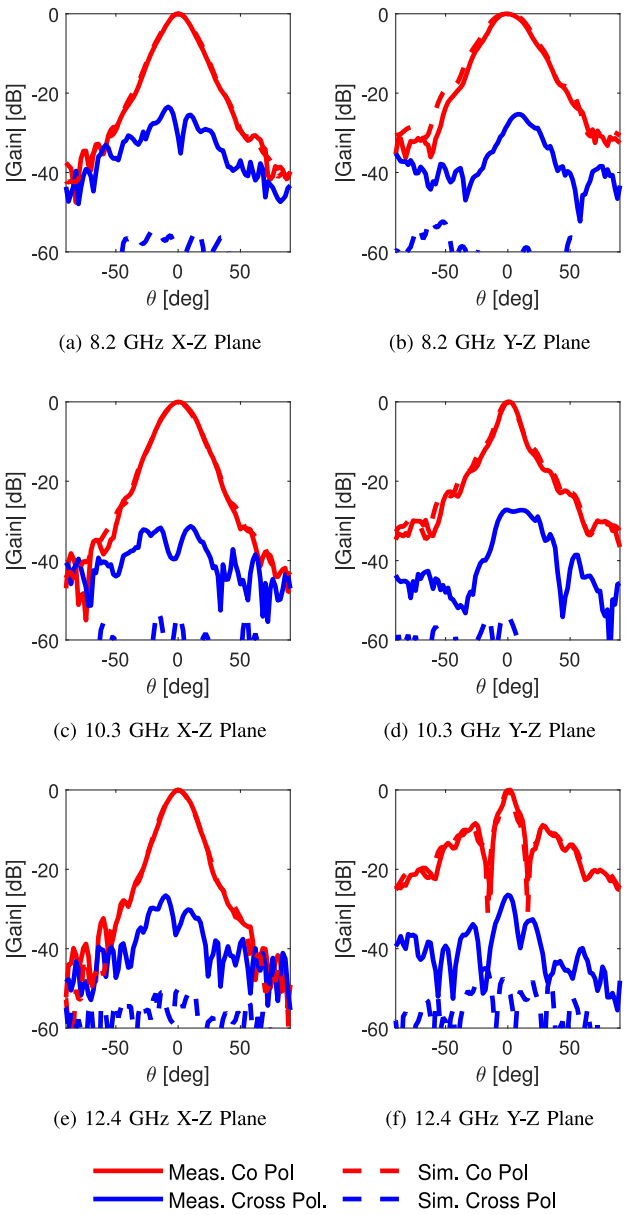

FIGURE 11. Measured and simulated normalized radiation patterns for linear transmit and port 1 receive.

measured and simulated data were taken at boresight. Here the measured linear peak gain was similar, but less than the expected values from simulation which is due to the reduced conductivity and increased surface roughness of all the 3D printed parts compared to the *idealized* stainless steel and aluminum models used in simulation. At 11 GHz the measured and simulated peak realized gain are very close and the simulated radiation efficiency was 95%. Like the port isolation in Fig. 9 (b) the measured cross polarization rejection Fig. 10 (b) was less than expected from simulation. This discrepancy in port isolation and cross-polarization rejection is attributed to the construction of the FDM printed horn, as measured cross-polarization rejection of DMLS feed without the horn performed equally to simulation. However, the measured linear cross-polarization rejection remained near 40 dB across the entire band.

The linearly polarized radiation patterns measured on port 1 are presented in Fig. 11 and shown the normalized gain across the band for co and cross polarization in the two main radiation pattern cuts as defined in Fig. 8 (c). Comparable results are shown for port 2 in Fig. 12. For both setups there is agreement between the measured and simulated co-polarized results, with the measured cross-polarization values

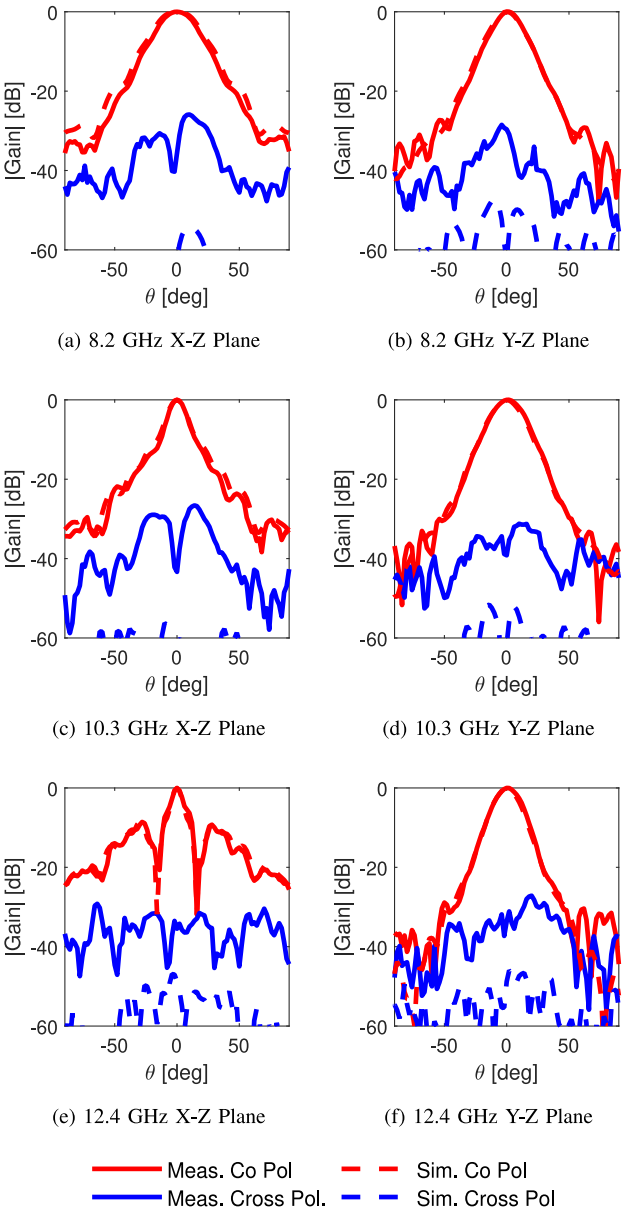

FIGURE 12. Measured and simulated normalized radiation patterns for linear transmit and port 2 receive.

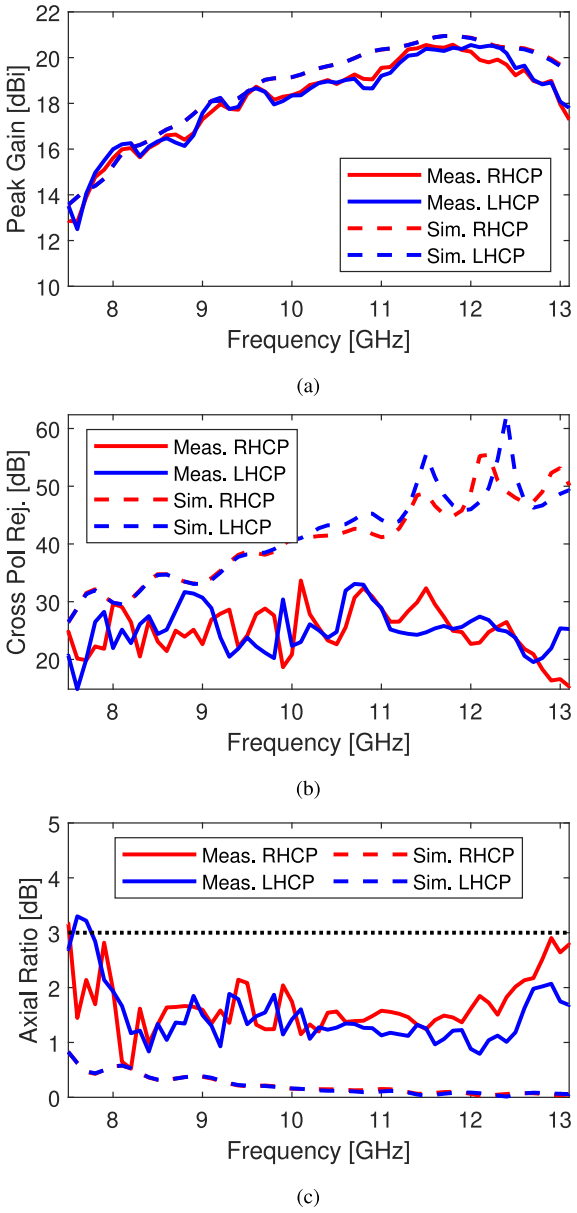

FIGURE 13. Measured and simulated circularly polarized transmit and receive (a) peak realized gain, (b) cross polarization rejection, and (c) axial ratio.

being higher than simulation which was expected based on the cross-polarization at boresight seen in Fig. 10 (b).

These linear results show that the this type of feed and antenna could be used for wide-band polarization division multiplexing, but the high port isolation and cross polarization rejection suggest that this antenna would be well suited for use with circularly polarized signals if the signals fed to the two ports were fed 90° out of phase since the two feed paths are the same phase length and feed the horn orthogonally. To measure the circularly polarized performance of the horn and feed it was fed using an off-the-shelf wide-band 90° hybrid (Pasternack PE2CP1150). The measurement setup was reconfigured using an Eravant quad-ridge dual polarized horn (SAV-0434031428-KFU5-QR) that was fed with an Eravant 90° hybrid to transmit either left hand or right hand circularly polarized (LHCP or RHCP) signals. Fig. 13 shows the measured and simulated: (a) peak gain, (b) cross polarization rejection, and (c) axial ration across the operating band all at boresight. The co-polarized peak gain showed good agreement between measurement and simulation with similar discrepancies to the linear results. As with the linear results, the measured circularly polarized cross polarization rejection was lower than expected, but still above 20 dB across the band. Finally, the measured axial ratio was less than 2 dB across the full WR 90 operating band.

Normalized radiation patterns across the band are shown for both LHCP transmit in Fig. 14 and RHCP transmit in Fig. 15 for two orthogonal radiation cuts. All patterns show good agreement between measurement and simulation with

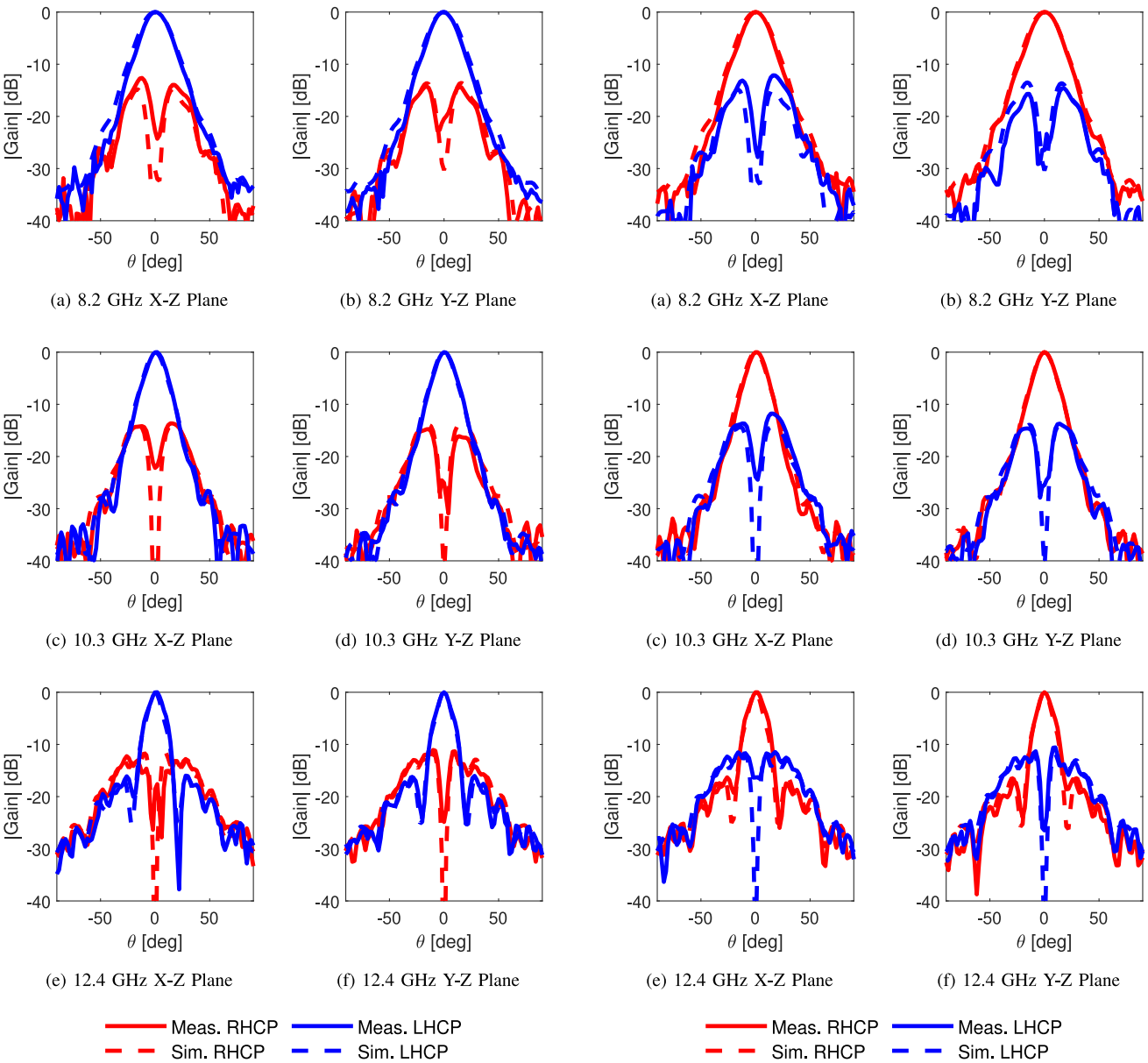

(a) 8.2 GHz X-Z Plane (b) 8.2 GHz Y-Z Plane

(c) 10.3 GHz X-Z Plane (d) 10.3 GHz Y-Z Plane

(e) 12.4 GHz X-Z Plane (f) 12.4 GHz Y-Z Plane

FIGURE 14. Measured and simulated normalized radiation patterns LHCP transmit.

(a) 8.2 GHz X-Z Plane (b) 8.2 GHz Y-Z Plane

(c) 10.3 GHz X-Z Plane (d) 10.3 GHz Y-Z Plane

(e) 12.4 GHz X-Z Plane (f) 12.4 GHz Y-Z Plane

FIGURE 15. Measured and simulated normalized radiation patterns RHCP transmit.

smooth and symmetrical radiation patterns which emphasizes the benefit of the dual and symmetric feeding structure over simpler methods of designing an OMT. For all patterns, the measured cross polarization rejection was less than simulated however, there is always a minimum in cross-polarization gain at boresight.

Finally, Table 1 provides a performance comparison is provided between the OMT in this work and other similar OMTs. Where this work provides a simple and inexpensive method of designing a balanced waveguide OMT with similar performance to more costly and complex topologies.

IV. CONCLUSION

Here a 3D printed waveguide feed and horn was presented that used a symmetric feed for each of the orthogonally polarized feed pairs to provide a symmetric radiation pattern across the operating band of 8.2 GHz to 12.4 GHz when considering the impedance match, axial ratio, and port isolation. The feed was a difficult geometry to CNC machine or metallize a plastic print, so it was 3D printed from stainless steel using selective laser sintering. The horn itself was FDM printed from PLA and metallized using aluminum tape. The setup provided a symmetric and balanced feed for each of the two orthogonal feed paths of the horn which provided port isolation better than 40 dB across the band which was evaluated for linear and circular polarization applications. The respective additive manufacturing methods used for the horn and feed were more cost effective than traditional CNC machining operations while continuing to affirm the effectiveness of these manufacturing methods to produce complex

TABLE 1. Comparison table between this work and select mm-wave dielectric lenses comparing far-field measured results at respective mid-band.

Ref.	Manufacturing Method	Topology	Peak Gain (dBi)	BW (GHz)	Isolation (dB)
This Work	3D printed FDM and DMLS		20.5	8.2–12.4	40
[1]	CNC Multi-Layer PCB	SIGGW*	10.0	27–36	50
[10]	DMLS	Turnstile	-	26.5–40	20
[13]	DMLS	Quad furcated profiled horn	19.5	10.5–13	56
[4]	CNC Machining	Waveguide OMT	-	30.5–36.5	50
[6]	CNC Machining	Turnstile	-	10–19.4	50
[17]	CNC Machining	Turnstile	-	10.5–13.5	30
[3]	CNC Machining	Turnstile	-	3.5–7.0	55

– Result not given in source

∗ Substrate-integrated groove gap waveguide

waveguide geometries while maintaining RF performance. This feed could be scaled for uses at other frequencies as the bandwidth of the device is only limited by the dimensions of the waveguide.

ACKNOWLEDGMENT

I. Goode is a recipient of the Ontario Graduate Scholarship from the Province of Ontario, Canada, the Ian M. Drum Scholarship at Queen's University, and NSERC PGS-D from the Government of Canada.

REFERENCES

[1] D. Cao, Y. Li, J. Wang, F. Sun, and L. Ge, "Millimeter-wave three-dimensional substrate-integrated OMT-fed horn antenna using vertical and planar groove gap waveguides," *IEEE Trans. Microw. Theory Techn.*, vol. 69, no. 10, pp. 4448–4459, Oct. 2021.

[2] S. Srikanth and M. Solatka, "A compact full waveguide band turnstile junction orthomode transducer," in *Proc. XXXth URSI General Assem. Sci. Symp.*, 2011, pp. 1–4.

[3] A. Tribak, J. L. Cano, A. Mediavilla, and M. Boussouis, "Octave bandwidth compact turnstile-based orthomode transducer," *IEEE Microw. Compon. Lett.*, vol. 20, no. 10, pp. 539–541, Oct. 2010.

[4] S. Jiang, Z. Chen, L. Min, and J. Dou, "A compact asymmetric waveguide orthomode transducer for millimeter-wave applications," *IEEE Microw. Compon. Lett.*, vol. 32, no. 1, pp. 17–20, Jan. 2022.

[5] C. Stoumpos et al., "Four-way orthomode waveguide power dividers: Subtractive and additive manufacturing," in *Proc. 15th Eur. Conf. Antennas Propagat. (EuCAP)*, 2021, pp. 1–5.

[6] J. L. Cano and A. Mediavilla, "Quasi-octave bandwidth in-phase three-layer platelet orthomode transducer using improved power combiners," *IEEE Microw. Wireless Compon. Lett.*, vol. 28, no. 12, pp. 1086–1088, Dec. 2018.

[7] S. Li, J. Han, and W. Cao, "Design of a Ku-band orthomode transducer," in *Proc. IEEE Int. Conf. Consum. Electron. Comput. Eng. (ICCECE)*, 2021, pp. 776–779.

[8] L. Schulwitz and A. Mortazawi, "Millimeter-wave dual polarized L-shaped horn antenna for wide-angle phased arrays," *IEEE Trans. Antennas Propag.*, vol. 54, no. 9, pp. 2663–2668, Sep. 2006.

[9] I. Goode and C. E. Saavedra, "3D printed X-band Orthomode transducer and conical waveguide horn antenna," in *Proc. IEEE Can. Conf. Elect. Comput. Eng. (CCECE)*, 2022, pp. 6–10.

[10] S. Chen, J. Li, Z. Xu, and T. Yuan, "A Ka-band wideband monolithically metallic 3-D printed turnstile junction orthomode transducer with shaped internal profile," in *Proc. IEEE/MTT-S Int. Microw. Symp. (IMS)*, 2022, pp. 676–679.

[11] J. Shen and D. S. Ricketts, "Compact W-band "swan neck" turnstile junction orthomode transducer implemented by 3-D printing," *IEEE Trans. Microw. Theory Techn.*, vol. 68, no. 8, pp. 3408–3417, Aug. 2020.

[12] F. Oktafiani, E. Y. Hamid, and A. Munir, "Wideband dual-polarized 3D printed quad-ridged horn antenna," *IEEE Access*, vol. 10, pp. 8036–8048, 2022.

[13] C. Stoumpos, J.-P. Fraysse, G. Goussetis, R. Sauleau, and H. Legay, "Quad-furcated profiled horn: The next generation highly efficient GEO antenna in additive manufacturing," *IEEE Open J. Antennas Propag.*, vol. 3, pp. 69–82, 2021.

[14] P. Allen, "The turnstile circulator," *IRE Trans. Microw. Theory Techn.*, vol. 4, no. 4, pp. 223–227, Oct. 1956.

[15] A. Navarrini and R. L. Plambeck, "A turnstile junction waveguide orthomode transducer," *IEEE Trans. Microw. Theory Techn.*, vol. 54, no. 1, pp. 272–277, Jan. 2006.

[16] S.-G. Park, H. Lee, and Y.-H. Kim, "A turnstile junction waveguide orthomode transducer for the simultaneous dual polarization radar," in *Proc. Asia Pac. Microw. Conf.*, 2009, pp. 135–138.

[17] J. L. Cano, A. Mediavilla, S. Dragas, and A. Tazón, "Novel broadband circular waveguide four-way power divider for dual polarization applications," *IEEE Microw. Wireless Compon. Lett.*, vol. 26, no. 2, pp. 98–100, Feb. 2016.

[18] I. Goode and C. E. Saavedra, "3D printed 18 GHz to 28 GHz horn antenna and gradient index of refraction lens," in *Proc. General Assem. Sci. Symp. Int. Union Radio Sci.*, 2021, pp. 1–4.

[19] I. Goode and C. E. Saavedra, "3D printed linearly polarized X-band conical horn antenna and lens," *IEEE Open J. Antennas Propag.*, vol. 3, pp. 549–556, 2022.

IAN GOODE received the B.A.Sc. degree in engineering physics with an Electrical Engineering sub-option from Queen's University in 2017, and the Ph.D. degree from the Department of Electrical Engineering, Queen's University in 2022. He was the Chief Technical Officer of Rover Design for the Queen's Space Engineering Team (QSET) from 2016 to 2018, where he oversaw the full redevelopment of QSET's Mars Rover prototype that competed with University Rover Challenge. His current research interests include lensed antennas and low-cost additive manufacturing methods for microwave systems. He has received multiple scholarships to support his graduate work, including the Ian M. Drum Scholarship, the Ontario Graduate Scholarship, and NSERC PGS-D. He is a recipient of the 2019 IEEE Kingston Section M.A.Sc Research Excellence Award and the 2021 URSI Young Scientist Award.

CARLOS E. SAAVEDRA received the B.Sc. degree in electrical engineering from the University of Virginia and the M.Sc. and Ph.D. degrees in electrical engineering from Cornell University, Ithaca, New York. He is a Registered Professional Engineer (P.Eng.) in Ontario, Canada. He is currently a Full Professor and the Head of the Department of Electrical and Computer Engineering, Queen's University, Kingston. On Sabbatical leaves, he has held visiting appointments with University of Navarra (Tecnun), San Sebastian, Spain, the Universidade Federal of Rio Grande do Sul, Brazil, and the University of Twente, Holland. He has served as the Co-Chair of the Natural Sciences and Engineering Research Council of Canada Discovery Grant Evaluation Group 1510 and has also served on grant review panels at the U.S. National Science Foundation. He is a former Associate Editor of the IEEE TRANSACTIONS ON MICROWAVE THEORY AND TECHNIQUES and a Guest Editor of the IEEE OPEN JOURNAL OF ANTENNAS AND PROPAGATION and the *IEEE Microwave Magazine*.